Advances in
Bridge Engineering

ORIGINAL INNOVATION

Open Access

Fatigue life prediction of stud shear connectors under corrosion-fatigue coupling effect

Lin Xiao, Yaxi Huang and Xing Wei*

*Correspondence:
we_star@swjtu.edu.cn

Department of Bridge Engineering, School of Civil Engineering, Southwest Jiaotong University, Chengdu 610031, China

Abstract

Based on the three-stage fatigue crack growth model, a corrosion fatigue life prediction method considering the coupling effect of corrosion and fatigue is proposed in this paper. In this case, stress factor amplitude was claimed considering the coupling effect of corrosion and fatigue. Three push-out tests in corrosion conditions were conducted to study the failure mode of studs. The crack propagation of studs, obtained through the push-out tests, was simulated in FRANC 3D to establish a library of adequate stress factor amplitude. According to the corrosion degree of the specimens, the corrosion dissolution rate formula was formed, and the corrosion fatigue life of the specimen was predicted. Results show that the error between the predicted and experimental values is approximately 25%.

Keywords: Stud, Corrosion fatigue, Crack propagation, Life prediction

1 Introduction

During the service life of the steel–concrete composite bridge, the combined action of the vehicle load cycle and corrosion results in the deterioration of bridge performance, and the structural performance of the bridge is seriously weakened (Wang et al. 2021; Jin DS 2021; Peng P 2020; Ma GL 2021). Researchers have considered corrosion and fatigue effects and found that the former significantly affects the fatigue performance of studs, which is shown evidently short fatigue life of studs (Wu, 2011). Theoretically, researchers have divided the entire life cycle of corrosion fatigue into three stages: corrosion pit initiation to nucleation life, corrosion pit propagation and crack propagation life, and fatigue crack propagation life (Goswami and Hoeppner 1997). Critical conditions of each stage change has been studied, resulting in such theoretical models as the critical depth of pitting (Huang, 2013), correlation model of crack growth rate, and stress intensity factor (Mcevily and Wei 1972). Amongst these conditions, there are two main schools of theoretical models of crack growth rate: the superposition model (Wei and Landes 1977) and the process competition model (Austen and Mcintyre 2013). The superposition model assumes that the crack growth rate of corrosion fatigue is the sum of the crack growth rates of stress corrosion

and fatigue damage. By contrast, the process competition model indicates that the crack growth rate of corrosion fatigue is determined by the higher crack growth rate of stress corrosion and fatigue damage. Literature (Kim et al. 1983) considered the modification of interaction based on the competition model, but its complex physical parameters and strict application conditions have resulted in a lack of wide applicability. Ge proposed an updated method of probabilistic life prediction of reinforced concrete structures based on the coupled deterioration mechanism of corrosion and fatigue (Ge and Kim 2021).

Researchers have also proposed a two-component corrosion fatigue crack propagation model in studying submarine pipeline steel's corrosion fatigue crack propagation (Cheng and Chen 2017). Zhen used the three-parameter model of steel wire fatigue crack growth in studying the corrosion fatigue life of steel wire, including the coefficient and index of crack growth, crack growth threshold, and stress intensity factor (Zheng et al. 2017). The empirical parameters of the model were determined through experiments and theoretical analysis, and the rationality of the theoretical model was verified. The three-parameter model is widely used in the field of corrosion fatigue crack propagation prediction (Liu et al. 2022). Han et al. predicted the corrosion fatigue life of cast steel butt weld based on this theoretical model, and the error was within 20% (Han et al. 2021). Beretta et al. studied the corrosion fatigue fracture of railway axles and used the observation of crack characterization as a basis to establish a set of high-precision corrosion fatigue life prediction systems by matching the corresponding crack growth rate models for different growth stages (Beretta et al. 2017).

For corrosion test research, S-N curves under the coupled action of corrosion fatigue through 19 RC test beams have been put forward to be the basis for corrosion fatigue life prediction (Wu et al. 2022). More specifically, the service life prediction formula of high-strength steel wires considering corrosion effects comes into being after a number of fatigue tests on six groups of steel wires with different corrosion degrees (Xue et al. 2020). Corrosion and fatigue effects have been considered more comprehensively in several tests on T-joint specimens, and a corrosion fatigue life calculation program for T-joints focusing on Miner's criterion has been proven effective (Liao et al. 2021). Xu carried out accelerated corrosion tests on headed stud shear connectors and found highly localized corrosion in the stud head (Xu et al. 2021). Ma established a fatigue life prediction model via several corrosion fatigues crack growth tests under different stress ratios and proposed a Bayesian Gaussian process-based corrosion fatigue damage assessment framework for bridge suspender wires (Ma et al. 2023).

Presently, research articles on corrosion-fatigue coupling life prediction are scattered, and the research on studs of composite bridges has remained insufficient. Previous studies on studs have often considered corrosion and fatigue separately. However, the actual service life of studs is substantially lower than the predicted value owing to the interaction between corrosion and fatigue. This paper considers this interaction and proposes the amplitude correction of the influential stress intensity factor considering the coupling effect. Moreover, the corrosion fatigue life of three specimens after corrosion fatigue loading is predicted numerically, and the rationality of the theory is verified by combining the experimental values.

2 Theory

2.1 Mechanical theory

Under the action of pure fatigue, the difference between the stress intensity factor corresponding to the maximum and minimum values of the alternating stresses on the material is called the stress intensity factor range Δ K, which is written as follows:

$$\Delta K = \Delta\sigma f(a) \tag{1}$$

where $\Delta\sigma$ represents stress amplitude, f is the geometric correction coefficient, and a is the crack length.

Linear elastic fracture mechanics defines da/dN as the crack propagation rate, where N represents the rounds of load cycles. The propagation rate of fatigue cracks shows a three-stage development law. (1) Crack propagation rate of the low rate zone (I) decreases rapidly with a decrease in the magnitude of the stress intensity factor. (2) The medium rate zone (II) da/dN has a good log linearity law with ΔK, which can be described by the Paris formula. (3) Lastly, da/dN in the high-speed rate zone (III) is considerably large to affect the fatigue life, thereby making it negligible. When the crack propagation rate is in the low rate region, correspondence between da/dN and ΔK can be described by the Paris formula (Eq. 2), where C and m are the basic parameters describing the crack propagation performance of the material, which are determined by experiments.

$$\frac{da}{dN} = C(\Delta K)^m \tag{2}$$

N can be obtained by integral:

$$N = \int_{a_0}^{a_c} \frac{da}{C\left(f(a)\Delta\sigma\sqrt{\pi a}\right)^m} \tag{3}$$

The Miner criterion describes the problem of material destruction under the successive action of variable amplitude cyclic loads. This criterion is expressed as follows:

$$\sum_{i=1}^{p} \frac{n_i}{N_i} \le 1 \tag{4}$$

Initial cracks of size a_0 extend to critical fracture size a_c after undergoing n_1, n_2, and n_3 cycles at stress levels $\Delta\sigma_1$, $\Delta\sigma_2$, and $\Delta\sigma_3$, respectively. After n_1 cycles under the action of stress level $\Delta\sigma_1$, crack size expands from a_0 to a_1, thereby leading to the following equation:

$$n_1(\Delta\sigma_1)^m = \int_{a_0}^{a_c} \frac{da}{C\left(f(a)\Delta\sigma\sqrt{\pi a}\right)^m} \tag{5}$$

Total damage is represented as follows:

$$D = D_1 + D_2 + D_3 = \frac{n_1}{N_1} + \frac{n_2}{N_2} + \frac{n_3}{N_3} \le 1 \tag{6}$$

In a corrosive environment, the definition of $\{da/dN\}_{cf}$ is the corrosion fatigue crack propagation rate, as shown in Fig. 1. Moreover, $\{da/dN\}_{cf}$ has the same trend as da/dN, the role of the corrosive medium generally accelerates the fatigue crack propagation rate and fatigue life prediction under both conditions is mainly based on the medium speed zone. Eqs. 3, 4, 5 and 6 indicate that the stress intensity factor amplitude during the expansion of corrosion fatigue cracks is the main parameter of the corrosion fatigue life prediction model.

2.2 Effective stress intensity factor amplitude under corrosion fatigue coupling

Different crack lengths $a_i(i=1,2,...n)$ under different stress amplitudes correspond to different effect force strength factor amplitude ΔK_{eff}. Several (a_i, ΔK_{eff}) value pairs are calculated using FRANC 3D. Given that (a_i, ΔK_{eff}) have a linear relationship, ΔK_{eff} corresponding to the length of any crack can be calculated by interpolation.

By dividing the crack propagation process into several time steps, the corrosion fatigue coupling effect will increase ΔK_{eff} in each substep, and the propagation in crack length caused by this enhancement effect further increases ΔK_{eff}. The effect of coupling on ΔK_{eff} in each substep is equivalent to the expansion of cracks from a_{i-1} to $a_{i-1}+\Delta a_{i-1}^{F}$ under fatigue. Δa_{i-1}^{C} indicates the increase in crack length caused by corrosion in the substep. Additionally, the correct ΔK_{eff}: ΔK_{eff}, K'_{eff} and K''_{eff} indicate the corresponding crack size of a_{i-1}, $a_{i-1}+\Delta a_{i-1}^{F}$, and $a_i+\Delta a_{i-1}^{F}+\Delta a_{i-1}^{C}$, respectively. When the crack length is $a_{i-1}+\Delta a_{i-1}^{F}$, the effective force strength factor amplitude is corrected as follows (see Fig. 2):

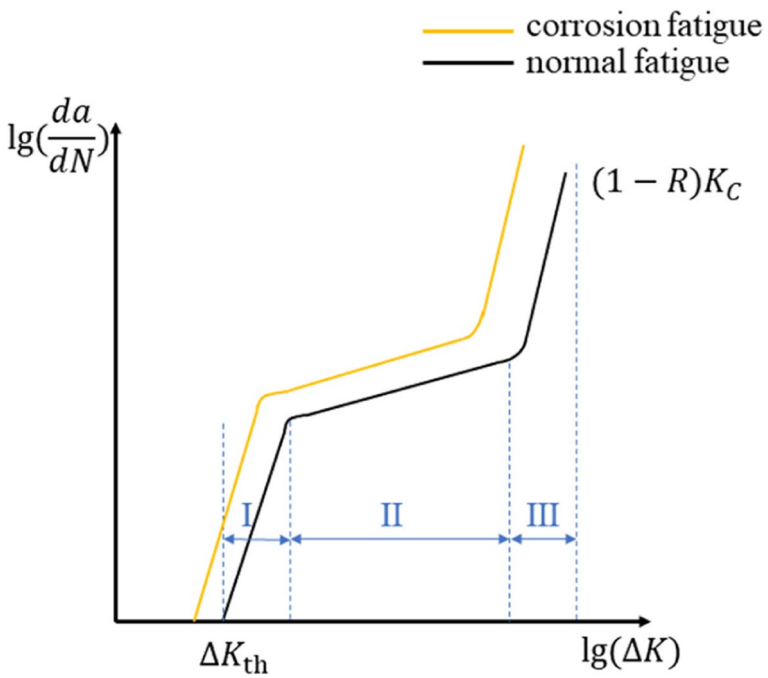

Fig. 1 Three-stage diagram of fatigue crack propagation

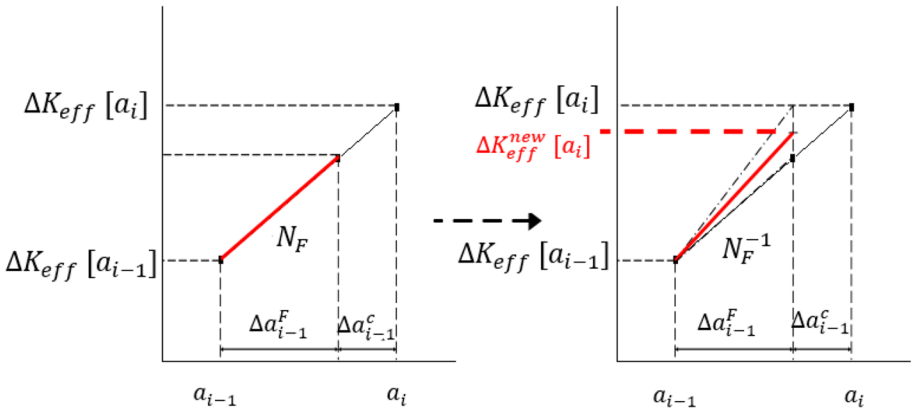

Fig. 2 Modification of effective stress intensity factor range

$$\Delta K_{eff}^{new} = \frac{\Delta K'_{eff} + \Delta K''_{eff}}{2} \tag{7}$$

2.3 Discrete substep method

On the basis of the Paris model of fatigue crack propagation under non-corrosive action, the corrosion fatigue process is decomposed into several discrete substeps: influence of corrosion and fatigue on crack propagation is comprehensively considered for each substep, life after corrosion fatigue coupling is obtained, and whole life under corrosion fatigue coupling is obtained by comprehensively superimposing each substep (Fig. 3). The specific implementation steps are as follows.

(1) Confirm basic parameters: stress amplitude $\Delta\sigma$, stress ratio R, stress intensity factor amplitude threshold ΔK_{th}, material parameters C, m, critical crack size a_c, and corrosion propagation rate function $f_C(t)$.

(2) When K_{eff} of the initial crack length a_{i-1} is less than ΔK_{th}, fatigue crack does not expand, and the expansion increment of the crack is determined only by the corrosion dissolution rate. Read a_{th} as crack extension threshold size, after Δt_{th} of corrosion time, crack size reaches a_{th}, and dissolution time is as follows:

$$\Delta t_{th} = f^{-1}(a_{th}) - f^{-1}(a_{i-1}) \tag{8}$$

After that, the fatigue crack begins to expand, calculated according to step (4).

(3) When K_{eff} of the initial crack length a_{i-1} is larger than ΔK_{th}, the crack begins to expand, and the corresponding crack expansion starts time is t_{i-1}. The following equation is derived according to the corrosion expansion rate function:

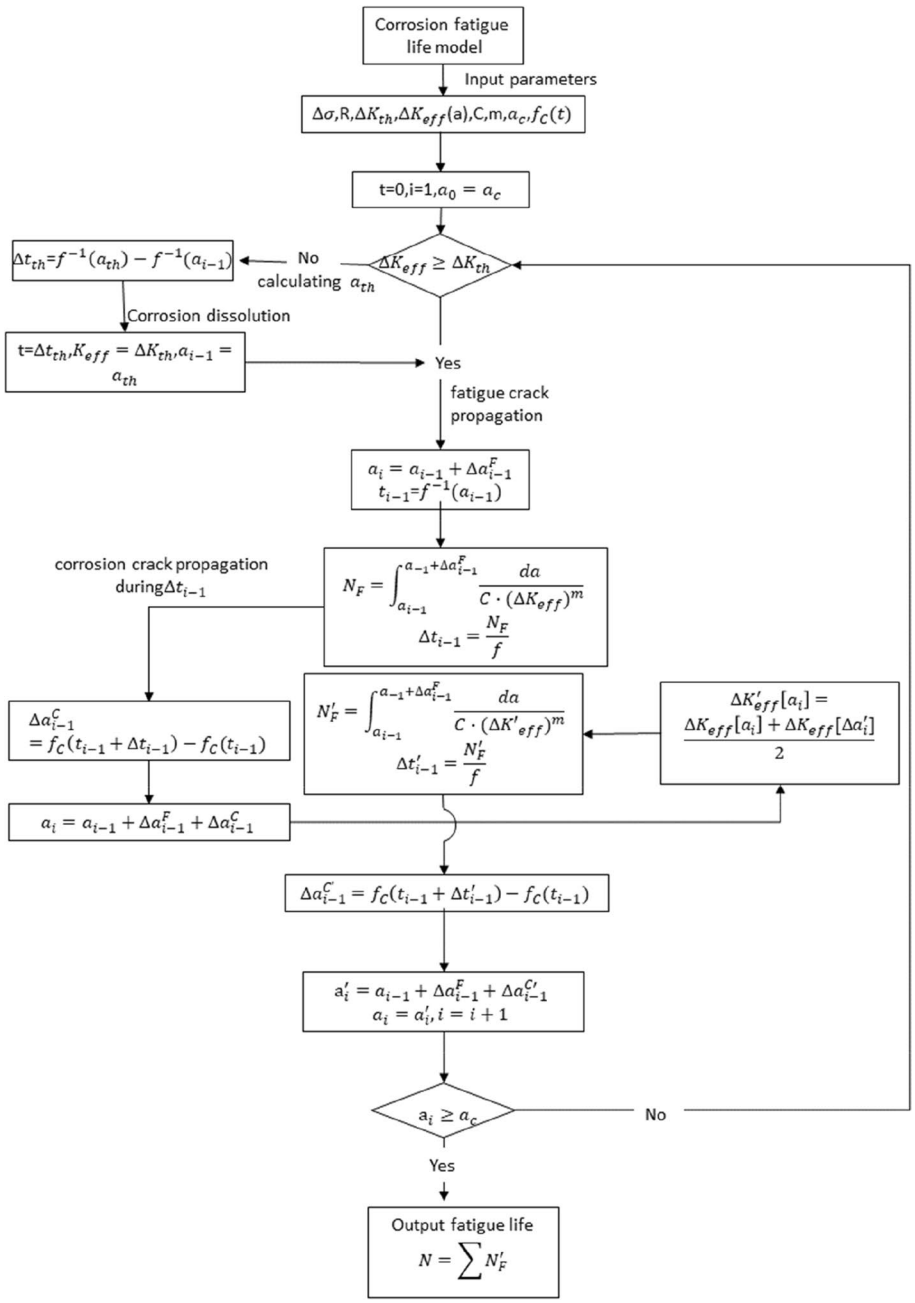

Fig. 3 Discrete substep calculation process

$$t_{i-1} = f^{-1}(a_i - 1) \tag{9}$$

Under fatigue, the substep crack extension length is Δa^F_{i-1}. Moreover, total crack length $\Delta a_{i-1} + \Delta a^F_{i-1}$ corresponds to the uncorrected effective force strength factor of $\Delta K'_{eff}$, with the required number of cycles and time represented respectively by the following equations:

$$N_F = \int_{a_{i-1}}^{a_{i-1}+\Delta a_{i-1}^F} \frac{1}{C \cdot \left(\Delta K'_{eff}\right)^m} da \tag{10}$$

$$\Delta t_{i-1} = \frac{N_F}{f} \tag{11}$$

The crack length increment caused by corrosion during period t_{i-1}~$t_{i-1}+\Delta t_{i-1}$ is expressed as follows:

$$\Delta a_{i-1}^C = f_C(t_{i-1} + \Delta t_{i-1}) - f_C(t_{i-1}) \tag{12}$$

(4) By considering the corrosion fatigue coupling effect, the modified effect force strength factor ΔK_{eff}^{new} replaces $\Delta K'_{eff}$, and the update life and step size are respectively expressed as follows:

$$N'_F = \int_{a_{i-1}}^{a_{i-1}+\Delta a_{i-1}^F} \frac{1}{C \cdot \left(\Delta K_{eff}^{new}\right)^m} da \tag{13}$$

$$\Delta t\prime_{i-1} = \frac{N\prime_F}{f} \tag{14}$$

The extended increment of the crack length caused by corrosion during period t_{i-1}~$t_{i-1}+\Delta t'_{i-1}$ is updated as follows:

$$\Delta a_{i-1}^{C\prime} = f_C(t_{i-1} + \Delta t\prime_{i-1}) - f_C(t_{i-1}) \tag{15}$$

Finally, the crack length expansion of the substep is expressed as follows:

$$\Delta a_{i-1} + \Delta a_{i-1}^F + \Delta a_{i-1}^{C\prime} \tag{16}$$

(5) Initial crack length of the next substep is the final crack length of the previous cycle substep. Calculation of steps (3) and (4) is repeated using the cyclic accumulation method, in which the corresponding load cycle number when the crack length reaches a_c and the total corrosion fatigue crack extension life can be obtained as follows:

$$N_{CF} = \sum N'_F \tag{17}$$

3 Corrosion fatigue push-out test

3.1 Experimental design and materials

Three sets of tests were designed for the corrosion-fatigue coupling test of studs. The specimen was introduced with reference to the standard in EC4, and a stud was arranged

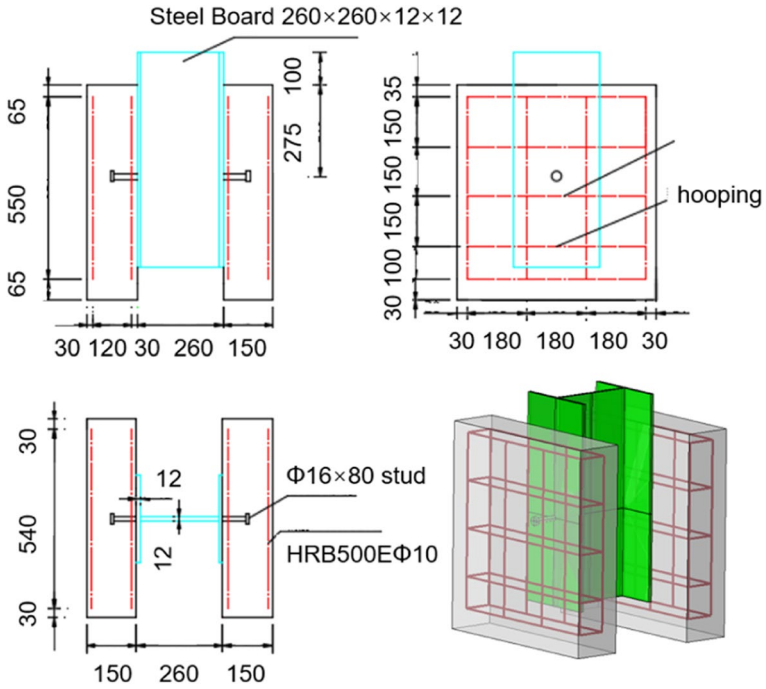

Fig. 4 Size of push-out specimen

Table 1 Test parameters

Name	Specimen set	Fatigue loads	Corrosive environment
Corrosion-fatigue test	CFP1	55%P_u	3.5%NaCl solution 400 mA
	CFP2	40%P_u	3.5%NaCl solution 400 mA
	CFP3	40%P_u	3.5%NaCl solution 100 mA

on one side (Fig. 4). The stud is 16 mm in diameter and 80 mm in height. The steel plate is 260 × 260 × 12 Q355 grade H-beam. Concrete slabs on both sides are 600 mm long, 150 mm wide, and 600 mm high, with a strength rating of C50. The stirrup diameter is 10 mm, lateral spacing is 180 mm, and vertical spacing is 150 mm. The experimental design is shown in Table 1. Each set of specimens contains two samples, and the results of subsequent tests are the average of two samples unless otherwise specified. Table 1 shows that the average ultimate bearing capacity of a set of corrosion-free and fatigue-free specimens obtained by the static force push test is 260 kN.

The specimens were immersed in 3.5% NaCl solution for 3 to 9 months (Fig. 5) for pre-corrosion treatment. Specimens in this paper were pre-soaked in 3.5% NaCl solution for 1 month before fatigue loading to simulate initial corrosion damage. Studies have shown that corrosion at the stud's root significantly impacts its service performance (Rong and Huang 2013). In order to prevent the steel plate and steel bar from being affected by corrosion, the steel plate and steel bar are polished and coated with anti-rust paint twice. In order to ensure that the solution can reach the peg surface quickly in the subsequent corrosion fatigue test, a hollow steel pipe with a diameter of 8 mm is set parallel to the corrosion pit when the template is built, and it is drawn out after the concrete reaches

Fig. 5 Immersion test

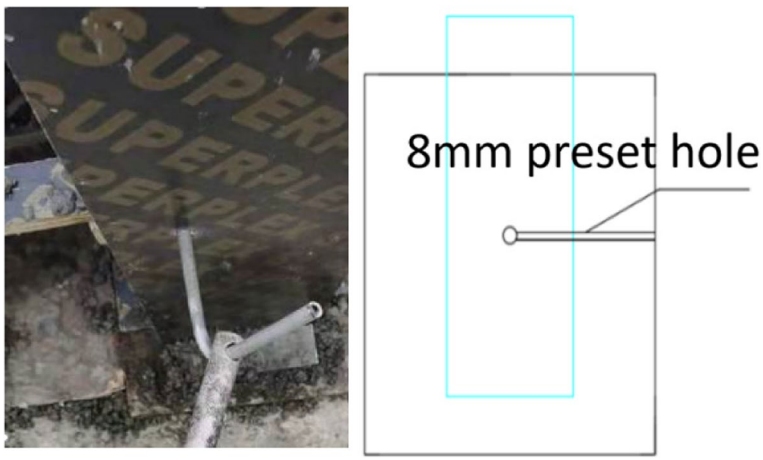

Fig. 6 Preset corrosion path at the root of the stud

the corresponding strength, so that the external corrosion solution can reach the corresponding peg interface faster, as shown in the figure. After the formwork pouring is completed, the specimen is covered with geotextile in the curing process to prevent the insufficient strength of the concrete specimen caused by low outdoor temperature (Fig. 6). To avoid the corrosion of the steel plate and steel bar affecting the force performance of the specimen, the steel plate and steel bar were brushed twice with antirust paint. During the fatigue test, the specimen was soaked in a 3.5%-NaCl solution and accelerated corrosion.

3.2 Load and test

After the pre-corrosion was completed, the solution in the corrosion box was replaced, and the specimen was hoisted together with the stainless steel corrosion box to the

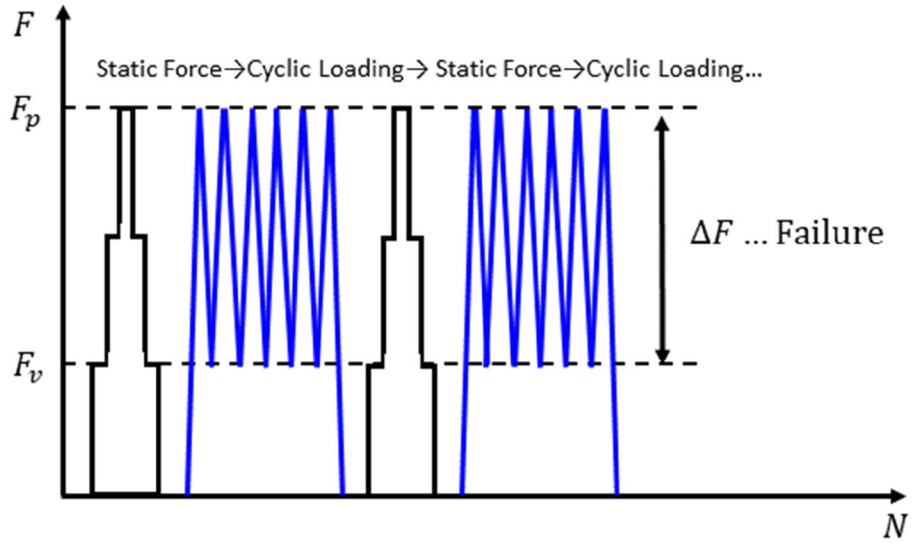

Fig. 7 Loading flow chart

bottom of the MTS (electronic universal testing machine). After the corresponding displacement meter was installed, the stainless steel wire mesh was placed in the stainless steel box, and the stainless steel wire mesh and reserved wire at the stud were connected to the DC power supply. Given that the placement of the insulating rubber plate will cause uneven force conduction between MTS and the specimen, and the steel beam of the specimen has been previously treated with the corresponding anti-rust insulation treatment, insulation measures were no longer taken between MTS and the specimen steel plate in this test. Load ratio η is the ratio of the fatigue load peak F_p to the ultimate bearing capacity P_{Rd} P_{Rd} of the specimen (Xiao, 2012), and fatigue load adopts a constant amplitude loading method with a loading frequency of 4 Hz. Conservatively assuming that the crack does not propagate when the stress is compressive; load peak and valley values are shown in Table 1. The minimum load F_v is constantly 26 kN. The loading flow chart is shown in Figs. 7 and the loading diagram of the corrosion fatigue group is shown in Fig. 8.

3.3 Specimen failure mode

After observing the damage on the specimen, the steel plate side was destroyed. Accordingly, evident rust marks can be clearly observed at the root of the stud, whilst the head was relatively rust-free (Fig. 9). Typical stud deformation in the specimen is shown in Fig.10. Note that the bending deformation of the stud is large after fatigue fracture, and bending deformations of CFP1, CFP2, and CFP3 are 11, 12 and 7 mm, respectively. The difference in the electrified rust rate makes the corresponding rust product rate different, thereby leading to different degrees of concrete support stiffness reduction, resulting in different degrees of bending deformation of specimen sets CFP2 and CFP3. Although the loading stress amplitude of CFP1 is larger than that of CFP2, the two bending deformations are close, and the corrosion rate of the two is at the same level. More corrosion time of CFP2 is given, and more corrosion and rust

Fig. 8 Loading diagram of the corrosion fatigue group

(a) CFP1 (b) CFP2 (c) CFP3

Fig. 9 Cross-section of the failed stud connector (steel plate side)

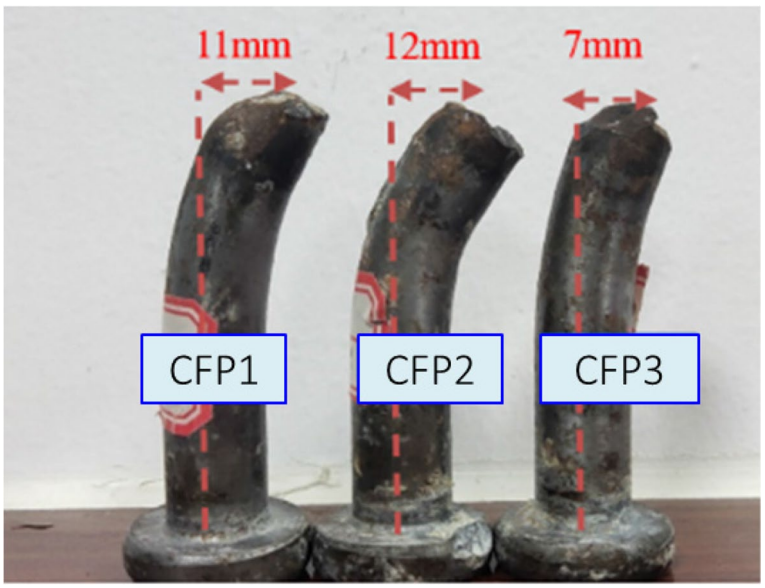

Fig. 10 Stud deformation diagram

products are on the stud root. The corresponding concrete support stiffness of CFP1 and CFPR is similar in their same corrosion rate. In the corrosion fatigue coupling effect, the stud connector may reduce the stiffness of concrete support owing to the generation of rust products. Additionally, force mode is converted from pure shear state to bent shear state, and the size of the stress amplitude and corrosion rate will affect the degree of bending deformation of the final stud joint.

The fracture morphology of the fatigue failure specimen was photographed using tungsten filament electron microscopy (JSM-IT500) to confirm the crack propagation path and fatigue fracture position of the stud in the test. The typical test piece fracture is shown in Fig. 11. Moreover, Fig. 11 shows an evident extension surface of shear fatigue at position 1, namely, a beach-like fatigue strip, a clear dividing line around the junction (position 2), a fatigue crack extension zone on the left and a microscopic feature of a metal plastic fracture similar to a tough socket fracture on the right. Similar microscopic features were also found in positions 3 and 4. Note that position 1 is the crack expansion area, position 2 is the junction of the crack expansion and fracture areas, positions 3 and 4 are the fracture area and the crack expansion surface is 'crescent-shaped.'

The stud failure mode in the corrosion-fatigue coupling test is stud shear fatigue failure. Fatigue crack originated from the compression side of the nail rod near the weld toe section and gradually developed into a crescent-shaped crack propagation area under cyclic shear stress. When fatigue crack or corrosion fatigue crack relatively expands, the uncracked area on the cross-section is broken under pull-shear combined stress, which differs from previous studies (Liu 2019). Accordingly, stud fatigue cracking is suggested to begin in the tensile area under the root and expands under tensile stress and breaks.

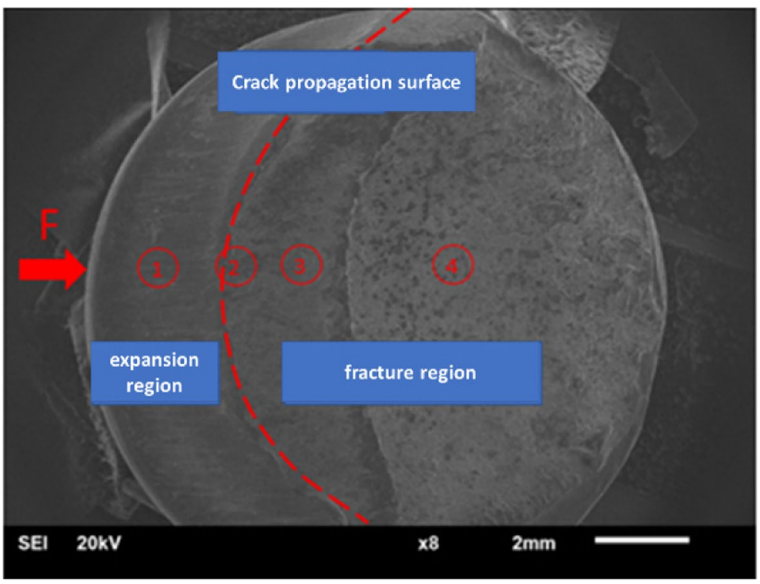

Fig. 11 Cross-section of the stud connector

4 Results and discussions

4.1 Stress intensity factor database based on Franc3D

This section only considers the change of the stress intensity factor of the crack tip and converts the three-dimensional crack propagation into a two-dimensional crack propagation consideration. To accurately solve the stress strength factor of the stud during crack propagation under cyclic load, the crack propagation path of the stud connector in the test should be accurately determined. Note that the fatigue crack of the stud connector in the corrosion fatigue test begins to expand from the compression side near the top plate and is eventually sheared under the action of the shear stress amplitude. Hence, type II stress strength factor amplitude is the effective force strength factor amplitude. On the basis of the plane crack propagation hypothesis, point A, located at the front of the crack, has the maximum value of the stress strength factor, which is declared as the reference point. The fatigue crack extension length variation is equivalent to the type II crack expansion direction. That is the crack length component change range in the shear force direction. Crack front point A extends from the initial crack length a_0 along the shear direction to the critical fracture crack length a_c.

Assuming that the proportion of the crack shape of the stud joint remains unchanged during the entire fatigue crack propagation process (Rajasankar and Iyer 2005), combined with the corrosion fatigue test results (Fig. 12), the shape of the crack front of the initial defect is taken as a 'half-moon' extension surface. Additionally, the initial crack was pre-placed 0.2 mm near the weld toe of the top plate of the steel plate. The center radial length of the initial crack is 0.2 mm, the maximum crack depth is 0.4 mm, the final fracture surface size crack center radial length is 4 mm, and the maximum crack depth is 8 mm. The fatigue crack propagation process is divided into 19 sub-steps, and the crack propagation length of each substep is 0.4 mm (Fig.13). the stress intensity factor of each substep is solved, and the amplitude library of the effective force strength factor is established.

FRANC3D (Fracture Analysis Code for 3D) crack analysis software and ABAQUS finite element software were used to solve the stress strength factor of stud connectors during fatigue expansion. Taking 1/2 of the specimens as the model object, the studs, steel beams,

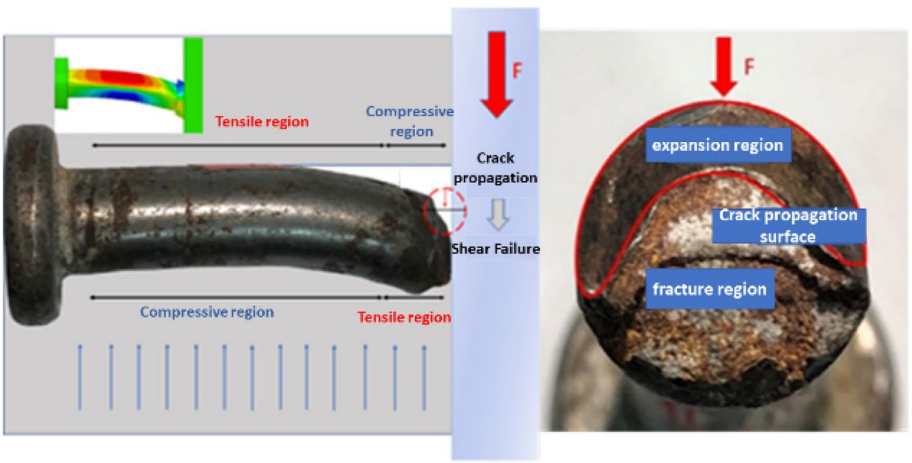

Fig. 12 Stud's mechanical behavior under corrosion-fatigue load

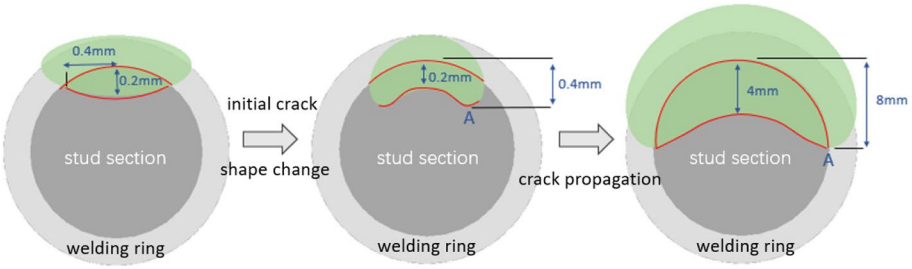

Fig. 13 Prefabricated initial crack and critical fracture crack size

and concrete units were simulated using solid unit C3D8R, and steel reinforcement was simulated by two-node three-dimensional truss T3D2 units. The surface contact between the steel beam and concrete is adopted. The normal use of the hard contact relationship and the tangent direction adopts the penalty function with a friction coefficient of 0.15. The outer side of the stud round head, the inner side of the ring between the rod head, and the inner side of the ring of the welding ring are in normal hard contact, and tangential frictionless contact relationships are adopted. The sides of the stud and the side of the welding ring are hard-contacted in the normal direction, and the tangential direction adopts a penalty function with a friction coefficient of 0.2. Using the stud root as a local model, the initial crack is prefabricated for the stud welding toe near the top plate, and the local model is substituted into the global model.

In this model, a 1/2 model is adopted for simulation, and the local grid details are divided for the key objects, such as bolts to achieve the effect of accurately simulating the force behavior of shear keys. In the test, contact relation is adopted to simulate the relationship between bolts and concrete. In order to ensure the accuracy and efficiency of calculation, the grid division of the parts where bolts and concrete contact are the same. The divided grid model is shown in Fig. 14. The model after the prefabricated crack is shown in Fig. 14 as well. The finite element model is first brought into ABAQUS for calculation, and the stress intensity factor value is obtained by FRANC3D. Regardless of the corrosion effect, the fatigue crack propagation process is divided into 19 sub-steps, and the crack extension length of each substep is 0.4 mm.

Moreover, the stress intensity factor of each substep is solved, and the amplitude library of the effective stress intensity factor under different stress ratios is established and combined with the simulated crack length, as shown in Fig. 15. The larger the load ratio for the same crack length, the greater the effective force strength factor. Under the same load ratio, the propagation of cracks will promote the amplitude of the effective force strength factor.

4.2 Corrosion dissolution rate function

The time course change function of the maximum corrosion depth of reinforced concrete beams after the accelerated galvanic corrosion test is expressed as follows (Sun et al. 2019):

$$d_{max} = A \cdot D\left(1 - \sqrt{1 - \rho_m}\right) + B \tag{18}$$

where A is the constant term (i.e. 1.6954), B indicates the initial corrosion depth when ρ_m is 0, d_{max} is the maximum corrosion depth, D is the cross-sectional diameter of the

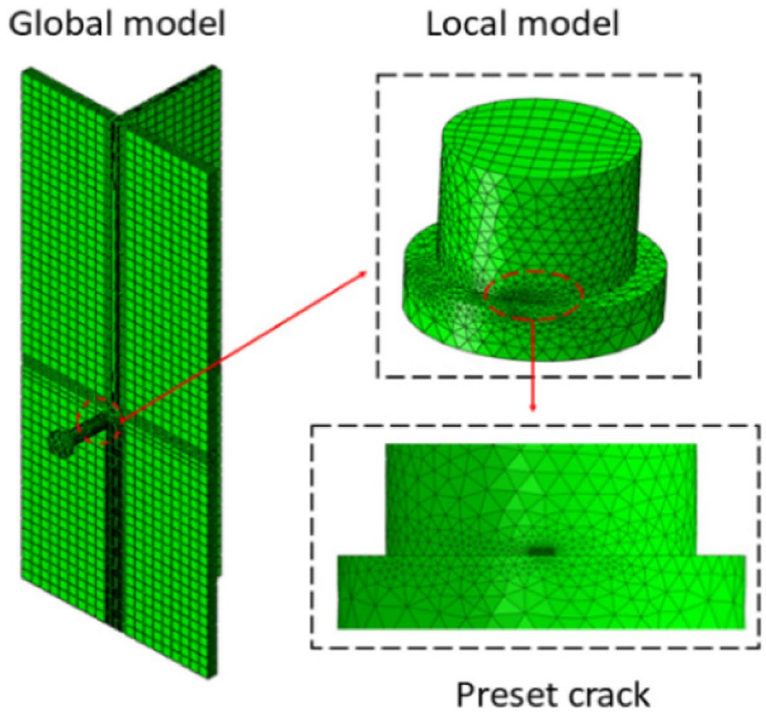

Fig. 14 Prefabricated stud model

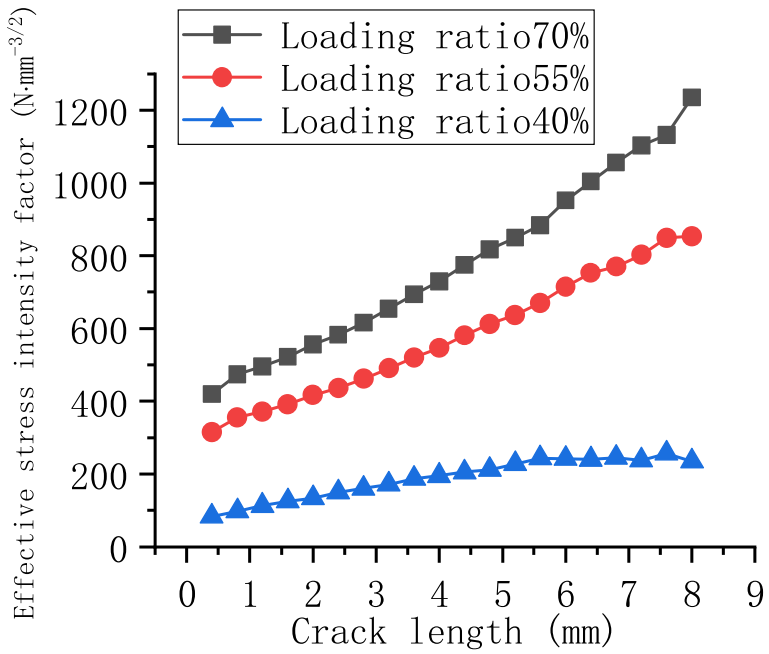

Fig. 15 Effective stress intensity factor range library

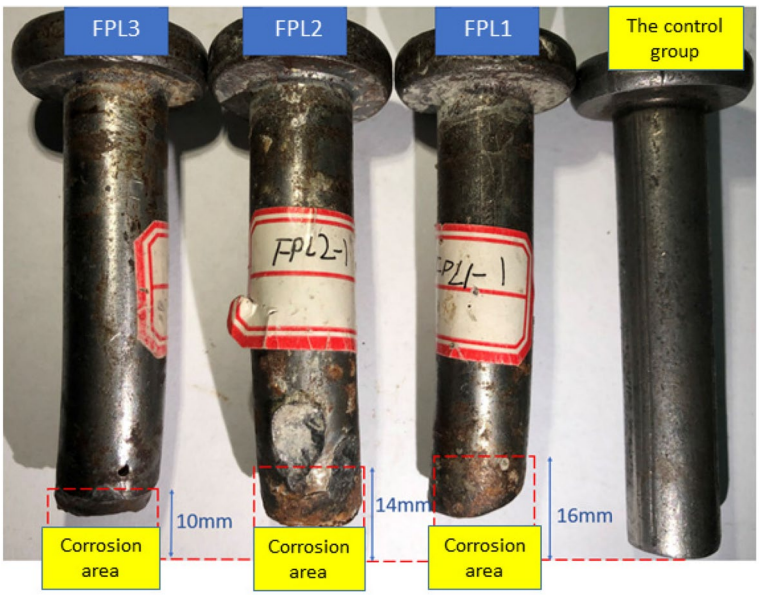

Fig. 16 Corrosion diagram of specimen

corrosive steel bar, and ρ_m is the corrosion rate. Let m_{loss} be the rust loss mass which can be calculated via the corrosion diagram of specimen shown in Fig.16, according to Faraday's law:

$$\rho_m = \frac{Z_{Fe} \cdot M_{Fe} \cdot I}{F \cdot m_{loss}} t \tag{19}$$

The corrosion dissolution rate function suitable for the test specimen is calculated as follows:

$$d_{max} = 27.1264\left(1 - \sqrt{1 - \rho_m}\right) + 0.4 \tag{20}$$

$$\rho_m = \frac{112I}{96490 \cdot m_{loss}} t \tag{21}$$

4.3 Corrosion fatigue life prediction

Programming is performed using Matlab based on the corrosion fatigue life prediction model theory in Section 2. Refer to BS7608 (BSI, 1993) to calculate the corrosion fatigue life of the three stud connectors by taking the C and m values of 5.21×10^{-13}N $\times$ mm$^{-3/2}$ and 3, respectively. Results include the crack propagation trends (Fig. 17) and life prediction values (Table 2) of the three specimens. Under the coupling effect of corrosion fatigue, crack propagation rate of the specimen maintains a high growth rate. Comparing the theoretical model prediction and test data, the estimated corrosion fatigue life is higher than the actual value but remains at a relatively close level. Detailed data are shown in Table 2. As the change of the propagation path is not considered when solving the stress intensity factor in the process of fatigue crack propagation, and the

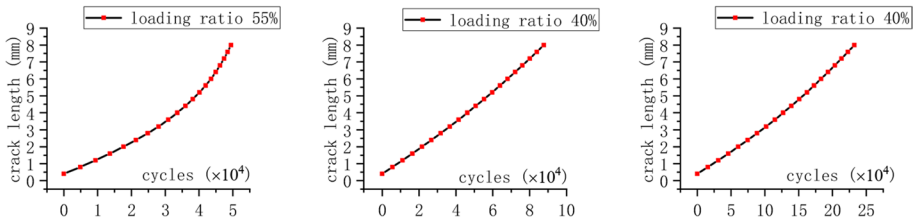

Fig. 17 Predictive value of corrosion fatigue crack life

Table 2 Predicted value of corrosion fatigue life

Specimen	Tests value	Calculating value	Errors
CFP1	40,954	49,462	20.7%
CFP2	67,400	87,696	30.1%
CFP3	180,000	232,539	29.2%

crack propagation path is constantly changing in reality, and there is a particular gap between the predicted corrosion fatigue life and the actual value.

5 Conclusions

(1) According to the modified amplitude of the effective stress intensity factor, a corrosion fatigue life prediction method considering the coupling effect of corrosion fatigue is proposed based on the Miner criterion and Paris formula.

(2) Under the action of corrosion-fatigue coupling, the failure mode of the specimen is the fatigue fracture of the stud. Damage originates from the compression side of the nail rod near the section of the weld toe. Shear crack expansion mainly occurs during the loading process, when the fatigue crack or corrosion fatigue crack relatively expands. The uncracked area on the cross-section is broken under the stress of the pull-shear combination.

(3) By presetting the initial crack, the stress intensity factor library of the shear joint under different stress ratios is established in FRANC3D. Crack length is consistent, and the load ratio is positively correlated with the effective force strength factor. Under the same load ratio, the crack propagation will increase the amplitude of the effective force strength factor.

(4) Lastly, a corrosion dissolution rate function suitable for shear joints is proposed based on existing research results combined with the test results. Hence, the life of shear joints under corrosion fatigue is predicted using MATLAB. The error between the experimental and predicted values is approximately 25%.

6 Nomenclature

ΔK Stress intensity factor amplitude.

$\Delta\sigma$ Stress amplitude.

ΔK_{eff} Effective stress intensity factor amplitude.

a Crack length.
da/dN Crack growth rate.
N Cycle of load.
C、m Material parameters.
N_{CF} Total corrosion fatigue crack propagation life.
ρ_m Corrosion rate.
Z_{Fe} Valence of iron.
F Faraday's electrolysis constant.
m_{loss} Weight loss of stud corrosion.
f Geometric correction factor.
a_c Critical fracture crack size.
a_0 Initial crack size.
ΔK_{th} Stress intensity factor amplitude threshold value.
K_C The critical stress intensity factor.
$\{da/dN\}_{cf}$ Corrosion fatigue crack growth rate.
R Stress ratio.
$f_C(t)$ Corrosion growth rate function.
B Corresponding initial corrosion depth when $\rho_m = 0$.
A Constant.
d_{max} Maximum corrosion depth.
M_{Fe} Molar mass of iron.
I Current density.

Acknowledgments
The authors acknowledge the financial support from the National Science Foundation of China (No.52178170, 52078424).

Authors' contributions
Lin Xiao proposed the prediction method; wrote the original draft. Yaxi Huang developed the calculating program; collected and analyzed the finite element calculation results. Xing Wei guided methodology development, substantially revised the draft and financial supports. The author(s) read and approved the final manuscript.

Funding
This study is supported by the National Natural Science Foundation of China (No. 52178170, 52078424).

Availability of data and materials
The data and materials in the current study are available from the corresponding author on reasonable request.

Declarations

Competing interests
The authors declare that they have no competing interest.

Received: 7 January 2023 Accepted: 15 February 2023
Published online: 02 March 2023

References

Austen IM, Mcintyre P (2013) Corrosion fatigue of high-strength steel in low-pressure hydrogen gas. Metal Science 13(7):420–428. https://doi.org/10.1179/msc.179.13.7.420
Beretta S, Sangalli F, Syeda J, Panggabean D, Rudlin J (2017) RAAI project: life-prediction and prognostics for railway axles under corrosion-fatigue damage. Procedia Structural Integrity 4:64–70. https://doi.org/10.1016/j.prostr.2017.07.010
British Standards Institution, BS7608-1993 Code of practice for Fatigue design and assessment of steel structures. London, 1993
Cheng A, Chen NZ (2017) Corrosion fatigue crack growth modelling for subsea pipeline steels. Ocean Eng 142:10–19. https://doi.org/10.1016/j.oceaneng.2017.06.057
Ge B, Kim S (2021) Probabilistic service life prediction updating with inspection information for RC structures subjected to coupled corrosion and fatigue. Eng Struct 238(4):112260. https://doi.org/10.1016/j.engstruct.2021.112260

Goswami T, Hoeppner DW (1997) Corrosion fatigue crack growth behavior of aircraft materials. J Mech Behav Mater 8(2)
Han QH, Wang X, Lu Y, Qi LG (2021) Corrosion fatigue life assessment method for cast steel and butt welds based on three-parameter Weibull distribution model. J Build Struct 42(02):213–220 https://doi.org/10.14006/j.jzjgxb.2020.c086
Huang XG (2013) Mechanism study of pit evolution and crack Propagatrion for corrosion fatigue, Doctor, Shanghai Jiao Tong University
Jin DS . (2021). Fatigue study of steel-concrete composite girder bridge considering the performance degradation, Master degree, Hefei University of Technology
Kim YH, Speaker SM, Wei RP, Manning SD (1983) Development of fatigue and crack propagation design and analysis methodology in a corrosive environment for typical mechanically-fastened joints. Volume 2. State-of-the-Art Assessment
Liao X, Qiang B, Wu J, Yao C, Li Y (2021) An improved life prediction model of corrosion fatigue for T-welded joint. Int J Fatigue 152(6):106438. https://doi.org/10.1016/j.ijfatigue.2021.106438
Liu D, Liu J, Huang F, Du LY, Peng WJ (2022) Corrosion fatigue crack growth prediction model based on stress ratio and threshold for marine engineering steel DH36Z35 in seawater. J Chin Soc Corrosion Protect 42(01):163–168
Liu YM (2019) Fatigue failure mechanism of steel-high performance concrete composite bridge deck with large-size U-ribs. Doctor, Southwest Jiaotong University
Ma GL (2021) Study on fatigue performance of steel-concrete composite beams with different stud arrangement. Master degree, Beijing Jiaotong University
Ma YF, Yu H, Wang GD, Wang L, Zhang JR, Lee DH (2023) Corrosion fatigue crack growth prediction of bridge suspender wires using Bayesian gaussian process. Int J Fatigue https://doi.org/10.1016/J.IJFATIGUE.2022.107377
Mcevily AJ, Wei RP (1972) In corrosion fatigue: chemistry. Mechanics and Microstructure
Peng P (2020) Long-term mechanical properties of steel-concrete composite beam subjected to corrosion and loading. Xiangtan University, Master Degree
Rajasankar J, Iyer NR (2005) A probability-based model for growth of corrosion pits in aluminium alloys. Eng Fract Mech 73(5). https://doi.org/10.1016/j.engfracmech.2005.10.001
Rong XL, Huang Q (2013) Experimental studies on static and fatigue behaviors of stud connectors for composite beams after corrosion. China Civil Eng J 34(02):15–20
Sun J, Ding Z, Huang Q (2019) Corrosion fatigue life prediction for steel bar in concrete based on fatigue crack propagation and equivalent initial flaw size. Constr Build Mater 195:208–217. https://doi.org/10.1016/j.conbuildmat.2018.11.056
Wu J, Yang J, Zhang R, Jin L, Du X (2022) Fatigue life estimating for chloride attacked RC beams using the S-N curve combined with mesoscale simulation of chloride ingress. Int J Fatigue 158:106751. https://doi.org/10.1016/j.ijfatigue.2022.106751
Wu JG . (2011). Durability of steel-concrete composite beams subjected to wet and dry cycling with composite solution. Master, Central South University
Wang LB , Qiu J, Huang L, Cao GH (2021) A calculation method of the ultimate bearing capacity of steel-concrete composite beam under the condition of stud corrosion. J Hunan City Univ (Natural Science) 30(03):17-20. https://doi.org/10.3969/j.issn.1672-7304
Wei RP, Landes JD (1977) Correlation between sustained-load and fatigue crack growth in high strength steels. Mater Res Stand 9(7):25–28
Xiao L (2012) Study of static and fatigue behavior of PBL shear connectors in steel-concrete composite structure. Doctor, Southwest Jiaotong University
Xu XQ, He DY, Zeng SW, He W, Tan HM, Yu ZW (2021) Effect of concrete cracks on the corrosion of headed studs in steel and concrete composite structures. Construc Build Mater. https://doi.org/10.1016/J.CONBUILDMAT.2021.123440
Xue S, Shen R, Chen W, Miao R (2020) Corrosion fatigue failure analysis and service life prediction of high strength steel wire. Eng Fail Anal 110:104440. https://doi.org/10.1016/j.engfailanal.2020.104440
Zheng XL, Xie X, Li XZ, Qian LQ , Shen YG (2017) Estimation model for steel wire crack propagation and its application in calculation of pre-corrosion fatigue life. China Civil Eng J 50(03):101–107

Publisher's Note